Heliyon 10 (2024) e28093

Contents lists available at ScienceDirect

Heliyon

journal homepage: www.cell.com/heliyon

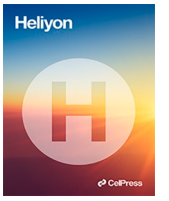

Research article

Butyrate attenuates the stemness of lung cancer cells through lysosome Fe^{2+}- and SLC7A11-mediated ferroptosis

Rui Bi [1], Lianyong Jiang [1], Rui Hu [1], Bohan Wen, Zhaolei Jiang [**], Hongtao Liu [***], Ju Mei [*]

Department of Cardiothoracic Surgery, Xinhua Hospital Affiliated to Shanghai Jiao Tong University School of Medicine, 1665 Kongjiang Road, Yangpu District, Shanghai, China

ARTICLE INFO

Keywords:
Butyrate
Ferroptosis
Cancer stem cells
SLC7A11
Lysosome Fe^{2+}

ABSTRACT

Cancer stem cells (CSCs) are considered key contributors to tumor progression, and ferroptosis has been identified as a potential target for CSCs. We have previously shown that butyrate enhances the ferroptosis induced by erastin in lung cancer cell, this study aimed to investigate the impact of butyrate on the progression of lung CSCs. To investigate these effects, we constructed a series of *in vitro* experiments, including 3D non-adherent sphere-formation, cytometry analysis, assessment of CSC marker expression, cell migration assay, and *in vivo* tumorigenesis analyses. Additionally, the influence of butyrate on chemotherapeutic sensitivity were determined through both *in vitro* and *in vivo* experiments. Mechanistically, immunofluorescence analysis was employed to examine the localization of biotin-conjugated butyrate. We identified that butyrate predominantly localized in the lysosome and concurrently recruited Fe^{2+} in lysosome. Moreover, butyrate reduced the stability of SLC7A11 protein stability in lung cancer cells through ubiquitination and proteasome degradation. Importantly, the effects of butyrate on lung CSCs were found to be dependent on lysosome Fe^{2+}- and SLC7A11-mediated ferroptosis. In summary, our results demonstrate that butyrate could induce the ferroptosis in lung CSCs by recruiting Fe^{2+} in lysosome and promoting the ubiquitination-lysosome degradation of SLC7A11 protein.

1. Introduction

Among the various types of cancer, lung cancer remains a formidable adversary with high morbidity and mortality rates [1]. In recent years, the emergence of new therapeutic strategies has provided promising avenues for combating this disease. One such strategy involves the manipulation of cellular metabolism to selectively target cancer cells [2]. Ferroptosis, an iron-dependent form of regulated cell death characterized by lipid peroxidation, has garnered considerable attention as a potential therapeutic avenue due to its unique mode of action and its implications in cancer progression [3].

Ferroptosis, characterized by the accumulation of lethal lipid peroxides resulting from iron-dependent reactions, is increasingly

* Corresponding author. Department of Cardiothoracic Surgery, Xinhua Hospital Affiliated to Shanghai Jiao Tong University School of Medicine, 1665 Kongjiang Road, Yangpu District, Shanghai, China.
** Corresponding author.
*** Corresponding author.
E-mail addresses: wojiangzhaolei@163.com (Z. Jiang), liuhtsmmu@sina.com (H. Liu), ju_mei63@126.com (J. Mei).
[1] These authors contributed to this work equally.

https://doi.org/10.1016/j.heliyon.2024.e28093
Received 6 October 2023; Received in revised form 11 March 2024; Accepted 12 March 2024
Available online 13 March 2024

recognized for its pivotal role in cancer cell death [3]. Notably, recent research has unveiled the complex interplay between ferroptosis and cancer stem cells (CSCs), a distinct subpopulation within tumors distinguished by their self-renewal and differentiation capabilities [4–6]. CSCs have emerged as crucial drivers of tumor progression and resistance to conventional therapies, sparking heightened interest in developing strategies to target CSCs and enhance the overall efficacy of cancer treatment [7]. The unique vulnerability of CSCs to ferroptosis offers a promising avenue for innovative therapeutic interventions. due to their heightened oxidative stress and iron metabolism, CSCs exhibit increased sensitivity to the lipid peroxidation and oxidative damage characteristic of ferroptosis [8]. Given this susceptibility, ferroptosis-inducing agents like erastin, have gained attention for their potential to selectively eliminate CSCs, thereby disrupting tumor growth and reducing the risk of recurrence [9].

Butyrate, a short-chain fatty acid, plays a pivotal role in various physiological processes within the human body [10]. Derived from the fermentation of dietary fiber by gut microbiota in the colon, butyrate serves not only as an essential energy source for colon lining cells but also contributes significantly to maintaining gut barrier integrity and regulating inflammation [11]. Its impact extends beyond the local environment, influencing immune responses, neurological functions, and even tumor progression [12–14]. The multifaceted roles of butyrate make it a promising subject of study in both gut health and overall human physiology. We previously demonstrated that butyrate enhances erastin-induced ferroptosis in lung cancer cells [15]. Other research has also unveiled the involvement of butyrate in ferroptosis [12,16–18]. Notably, prior studies have shown that butyrate can regulate the differentiation of human periodontal ligament stem cells [19], mesenchymal stem cells [20], and neural stem/progenitor cell [21]. Considering that the expression of genes involved in normal stem cell development is usually reinstated in tumors [22], we speculated that butyrate might hold critical roles in CSC progression. Building on these insights, we sought to explore the effects of butyrate on the progression of lung CSCs and its potential role in ferroptosis induction. Employing a comprehensive approach, we conducted both *in vitro* and *in vivo* experiments to elucidate the impact of butyrate on lung CSCs. *In vitro* investigations encompassed 3D non-adherent sphere formation, cytometry analysis, and the assessment of CSC marker expression. Additionally, we conducted *in vivo* tumorigenesis analyses to evaluate the effects of butyrate in a physiological context. Beyond examining butyrate's direct effects on CSCs, we delved into its role in chemotherapeutic sensitivity using both *in vitro* and *in vivo* models.

To gain mechanistic insights into the mode of action of butyrate, we conducted immunofluorescence analyses to track the localization of biotin-conjugated butyrate. Our findings unveiled that butyrate predominantly localized within lysosomes, simultaneously recruiting Fe^{2+} into these organelles. Furthermore, our investigation uncovered a novel regulatory pathway involving the ubiquitination and lysosome degradation of SLC7A11 protein, a pivotal mediator of ferroptosis resistance. This finding underscores the multifaceted impact of butyrate on the cellular machinery governing ferroptosis in lung cancer cells. Ultimately, these insights have the potential to pave the way for innovative therapeutic strategies targeting lung cancer, particularly focusing on the critical CSC population, through the manipulation of ferroptosis pathways.

2. Materials and methods

2.1. Cell culture and reagents

The lung cancer cell lines A549 and H1299, and normal bronchial epithelial BEAS2B cells were cultured in RPMI1640 media (Cat # 12633012, GIBCO BRL, Grand Island, NY, USA) supplemented with fetal bovine serum (Cat # A5669401, FBS, GIBCO BRL) and 1% antibiotics (Penicillin and Streptomycin) (Cat #C0222, Beyotime, Beijing, China). The cells were maintained in a humidified atmosphere at 37 °C with 5% CO_2. Necrosis inhibitor Nec-1 (APExBIO, Cat # A4213), apoptosis inhibitor Z-VAD-FMK (APExBIO, Cat # A1902), and ferroptosis inhibitor Fer-1 (APExBIO, Cat # A4371) were purchased from APExBIO (Houston, USA). Butyrate (Cat #S1999) was purchased from Selleck Chemicals and exists in the form of sodium salts.

2.2. RT-qPCR

Total RNA was extracted from A549 and H1299 cells using TRIzol reagent (Cat #T9424, Sigma-Aldrich, St. Louis, MO, USA). cDNA synthesis was performed using a reverse transcription kit (Cat # 11119ES60, Yeasen, Shanghai, China). Real-time quantitative PCR (RT-qPCR) was then performed employing specific primers with Hieff UNICON® Universal Blue qPCR SYBR Green Master Mix (Cat # 11201ES03, Yeasen) to evaluate the expression of target genes. GAPDH served as the internal control. The sequences of RT-qPCR primers were listed as below: Nanog-forward, 5′- GCAGGCAACTCACTTTATCC -3′, Nanog-reverse, 5′- CCCACAAATCACAGGCATAG -3'; ALDH1-forward, 5′- AGCCTTCACAGGATCAACAGA -3′, ALDH1-reverse, 5′- GTCGGCATCAGCTAACACAA -3'; GAPDH-forward, 5′- CTTAGTTGCGTTACACCCTTTCTTG -3′, GAPDH-reverse, 5′- CTGTCACCTTCACCGTTCCAGTTT -3'; E-cadherin-forward, 5′- ATGGCTTCCCTCTTTCATCTCCTG -3′, E-cadherin-reverse, 5′- CATAGTTCCGCTCTGTCTTTGGCT -3'; Vimentin-forward, 5′- GGGAGGCCCACGTATGGCGCCTCTC -3′, Vimentin-reverse, 5′- GAGAGGCGCCATACGTGGGCCTCCC -3'. IRP2-forward, 5′- TTATCTTGCCTCTCCACCCTTAGT -3′, IRP2-reverse, 5′- CACCGTTTATTCCCCATTTCTATT -3'. TfR1-forward, 5′- ATAGGAGATACCAGGTTGAAAGAC -3′, TfR1-reverse, 5′- GGAAGAAACAAAAATAACAAAGAA -3'. DMT1-forward, 5′- AAACCGGAACAATAAGCAGGAAGT -3′, DMT1-reverse, 5′- GATGGCAATAGAGCGAGTCAGAAC -3'. Ferritin-forward, 5′- GTTAGTTCAGAGGTGAGTTTTGTT -3′, Ferritin-reverse, 5′- GAGTGTATGACTGTTATGAGGTGG -3'.

2.3. Western blot

Protein lysates from A549 and H1299 cells were prepared using RIPA lysis buffer (Cat #P0013B, Beyotime). The protein

concentrations were quantified using the BCA protein assay kit (Cat #P0009, Beyotime). Equal amounts of protein were separated by SDS-PAGE, transferred to PVDF membranes (Cat # 24937-79-9, Sigma), and subjected to immunoblotting with primary antibodies against specific proteins of interest. HRP-conjugated secondary antibodies (Cat # A0208, Beyotime) were employed for detection, and protein bands were visualized using chemiluminescence (Cat # 180–501, Tanon, Shanghai, China). The detailed information about antibodies were listed as below: Nanog (Cat#14295-1-AP, Proteintech, Wuhan, China), ALDH1 (Cat#15910-1-AP, Proteintech), GAPDH (Cat#60004-1-Ig, Proteintech), E-cadherin (Cat# 20874-1-AP, Proteintech), Vimentin (Cat# 10366-1-AP, Proteintech), SLC7A11 (Cat# 26864-1-AP, Proteintech). The original uncropped images were shown in Supplementary data.

2.4. Cell viability assay

A549, H1299, and BEAS2B cells were treated with butyrate at the concentration of 0, 1, 5, and 25 μM for 48 h, and cells were seeded onto a 96-well plate at 5×10^3 cells per well. The CCK-8 assay (Cat # AWC0114a, Abiowell, Changsha, Hunan, China) was used to assess the cell viability referring to the product instructions. Briefly, PBS was added to each well together with 10 μL per well of CCK-8 reagent, and the plate was then incubated for 4 h at 37 °C. Subsequently, the measurement of the optical density (OD) value at 450 nm was performed with a microplate reader (Heales, China).

2.5. Immunofluorescence (IF) and Fe^{2+} localization analysis

Immunofluorescence staining was conducted to visualize the intracellular localization of biotin-conjugated butyrate. The localization of Fe^{2+} was assessed using specific fluorescent probes (FerroOrange, DOJINDO, Cat #F374). Subsequently, confocal microscopy was employed to capture the subcellular distribution of butyrate and Fe^{2+}.

2.6. 3D non-adherent sphere-formation

A549 and H1299 cells were cultured under non-adherent conditions to form 3D spheroids for 10 days using media without serum and including reagents as previously depicted [6]. The effect of butyrate on the morphology and size of these spheroids was subsequently assessed. To investigate the effects of butyrate on the viability of lung CSCs, spheres derived from lung cancer cells were enzymatically dissociated and re-seeded into 96-well plates. Following cell adhesion, butyrate was added to cells to incubate for 48 h. Cell viability was then measured through MTT analysis.

2.7. Cytometry analysis

Flow cytometry was conducted to analyze the ratio of CD133+ subpopulation in A549 and H1299 cells. Briefly, cells were washed in PBS, re-suspended with anti-CD133-PE (Cat # 940373, BD Biosciences, USA), and then incubated at 4 °C for 30 min in the dark. The labeled cells were washed using PBS and analyzed using a flow cytometer (BD, USA). The negative fraction was determined using appropriate isotype control. 20,000 cells were collected to analyze the impact of butyrate on the proportion of CSCs within the cell population.

2.8. ALDH activity detection

The activity of aldehyde dehydrogenase (ALDH), a commonly used CSC marker, was measured using an Aldehyde Dehydrogenase Activity Test Kit (Cat # MAK082-1 KT, Merck Millipore). Alterations in ALDH activity in response to butyrate treatment were then quantified for analysis.

2.9. Protein stability analysis

The stability of SLC7A11 protein in A549 and H1299 cells was assessed following butyrate treatment and CHX treatment (5 μg/ml, Sigma) at different time-points. Ubiquitination and lysosome degradation pathways associated with SLC7A11 protein turnover were also investigated using Western blot analysis.

2.10. Lentivirus package and cell infection

Lentiviral particles carrying SLC7A11 overexpression vector or empty control vector were generated for subsequent cell infection. A549 and H1299 cells were infected with lentiviral particles to modulate gene expression and construct stable-infected cell line after being screened using puromycin (1 μg/ml, Sigma).

2.11. Transwell migration and invasion analysis

Transwell chambers with or without matrigel (BD Pharmingen, San Diego, CA, USA) were used to assess the migration and invasion capabilities of A549 and H1299 cells, respectively, following the protocols as previously depicted [23].

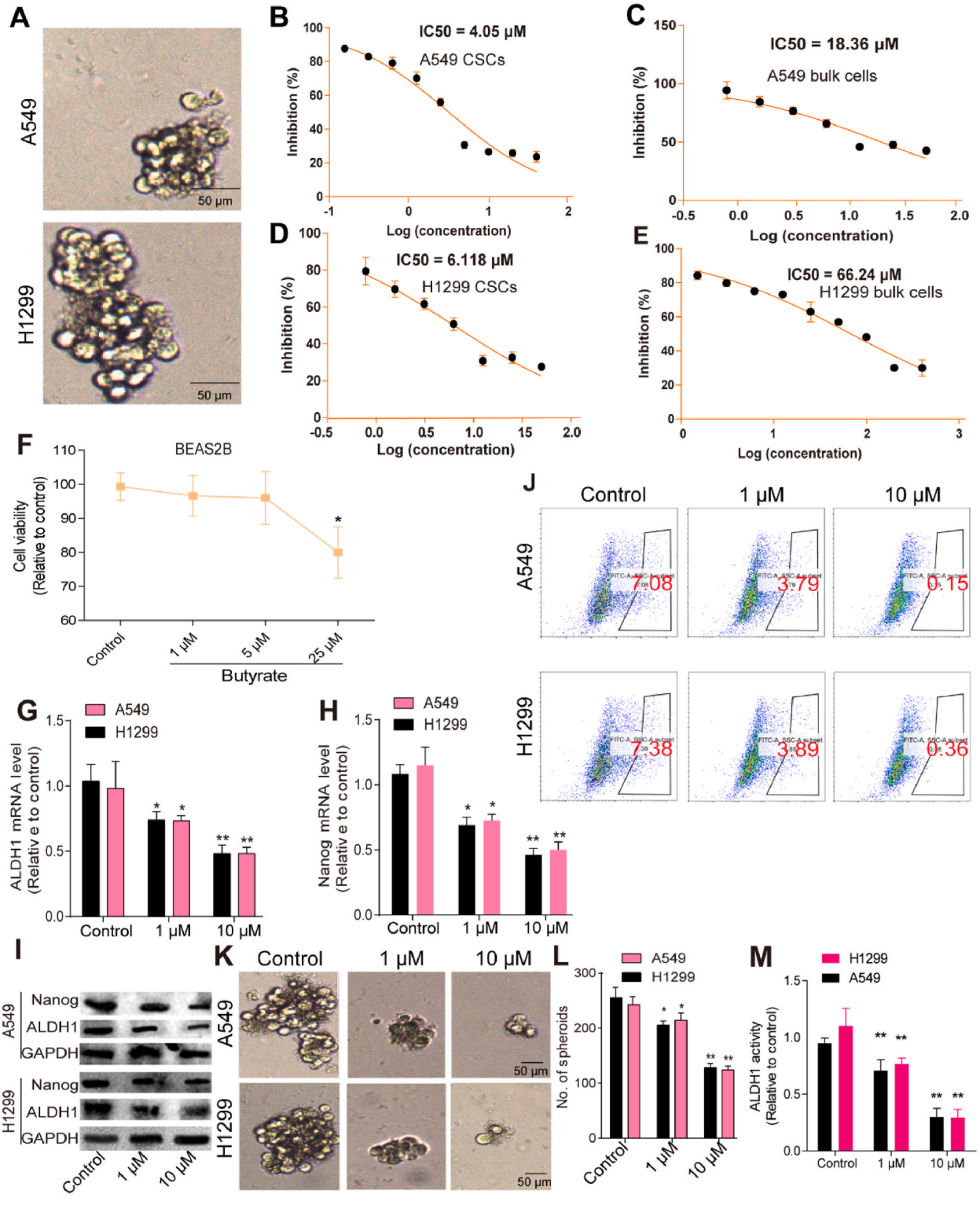

(caption on next page)

Fig. 1. Butyrate preferably suppresses the viability of lung CSCs and stemness of lung cancer cells. (A) The represented images of spheres formed by A549 and H1299 cells. (B and C) The IC50 values of butyrate were calculated in A549 CSCs and bulk cells. (D and E) The IC50 values of butyrate were measured in H1299 CSCs and bulk cells. (F) The viability of BEAS2B cells was evaluated after being treated with different concentrations of butyrate for 48 h. (G–I) The expression of stemness markers was detected in A549 and H1299 cells with or without the treatment of different concentrations of butyrate. (J) CD133+ subpopulation in A549 and H1299 cells was examined after being the treatment of different concentrations of butyrate. (K and L) The sphere size and number were evaluated in the cells depicted in (G). (M) ALDH1 activity was measured in the cells described in (G). *P < 0.05, **P < 0.01 vs control group.

2.12. In vitro chemotherapeutic sensitivity analysis

The sensitivity of A549 and H1299 cells to cisplatin was assessed *in vitro*. Cells were treated with varying concentrations of cisplatin with or without butyrate treatment, and cell viability was determined using cell viability analysis.

2.13. ELDA: Extreme Limiting Dilution Analysis

All animal experiments were obtained the approval of the Ethics Committee for Animal Experimentation of Shanghai Jiao Tong University. Extreme limiting dilution analysis was employed to estimate the frequency of CSCs within A549 and H1299 cell populations. This technique facilitated the identification of CSC-enriched subpopulations and their response to butyrate treatment. In a concise manner, A549 and H1299 cells were pretreated with butyrate for 72 h and subsequently injected into 6-week-old nude mice (s.c) at concentrations of 1×10^7 cells per mouse, 1×10^6 cells per mouse, 1×10^5 cells per mouse, respectively. After two weeks, the frequency of CSCs was determined using ELDA analysis.

2.14. In vivo chemotherapeutic sensitivity analysis

In vivo experiments were conducted to evaluate the response of tumor xenografts derived from A549 cells to chemotherapeutic treatment. A549 cells were subcutaneously injected into one side of 6-weeks old BALB/c nude mice. Once the tumor volume reached approximately 100 mm^3, the mice were randomly divided into the solvent group, 5 mg/kg cisplatin group, 10 mg/kg butyrate group, and 5 mg/kg cisplatin+10 mg/kg butyrate group. The drugs were administered intraperitoneally every three days. Tumor size was measured at three-day intervals using Vernier calipers and converted to tumor volume (TV) using the formula: $TV\ (mm^3) = (a \times b^2)/2$, where a and b represent the largest and smallest diameters, respectively. After 21 days of administration, the tumors were excised, and the weight of each tumor was measured and documented.

2.15. In vivo metastatic ability assay

The *in vivo* metastatic potential of A549 and H1299 cells was evaluated as follows: 1×10^6 cells were injected into mice (i.v) and subsequently treated with butyrate for a duration of two weeks. Following this period, the lung tissues were harvested and subjected to HE staining to observe and analyze the presence of the lung metastatic nodes.

2.16. Statistical analysis

Data from various experiments were presented as mean ± standard deviation (SD) and analyzed using appropriate statistical tests. Student's t-test or analysis of variance (ANOVA) followed by post-hoc tests were employed to determine statistical significance. P-values below 0.05 were considered statistically significant.

3. Results

3.1. Butyrate preferably suppresses the viability of lung CSCs and stemness of lung cancer cells

We initially collected lung CSCs through 3D non-adherent sphere-formation analysis (Fig. 1A) and observed a notable preference of butyrate treatment for suppressing the viability of lung CSCs compared to that of lung cancer cells (Fig. 1B – 1E). Importantly, it is noteworthy that butyrate exhibits toxicity to normal bronchial epithelial BEAS2B cells at a concentration of 25 μM (Fig. 1F), underscoring its comparatively lower toxicity to normal cells. We further confirmed this effect by examining the effects of butyrate on lung cancer cell stemness. It was consistently found that butyrate significantly diminished the stemness of lung cancer cells, as evidenced by the reduction in the expression of CSC markers (Fig. 1G – 1I), the CD133+ cell subpopulation with stemness (Fig. 1J), the sphere-formation ability (Fig. 1K and L), and ALDH activity (Fig. 1M).

3.2. Butyrate inhibits the migration and invasion ability of lung cancer cells

We further assessed the effects of butyrate on the migration and invasion abilities of lung cancer cells, recognizing the significant contribution of CSCs to cancer progression. The transwell migration assays revealed a substantial impairment in the migration ability of lung cancer cells following butyrate treatment (Fig. 2A and B). Consistently, butyrate treatment notably suppressed the invasion

ability of lung cancer cells (Fig. 2A and C). Moreover, butyrate treatment demonstrated a considerable attenuation of the epithelial-mesenchymal transformation (EMT), characterized by a decrease in the expression of mesenchymal marker and an increase of epithelial marker (Fig. 2D - **2F**), potentially influencing key processes associated with cancer cell behavior and metastatic potential.

3.3. *Butyrate attenuates the stemness of lung cancer cells in vivo*

In our *in vivo* experiments employing tumor xenograft models derived from A549 and H1299 cells pre-treated with butyrate for 72 h, we illustrated that butyrate treatment resulted in a reduction in the tumor formation ratio (Fig. 3A and B , Fig. 3E and F).

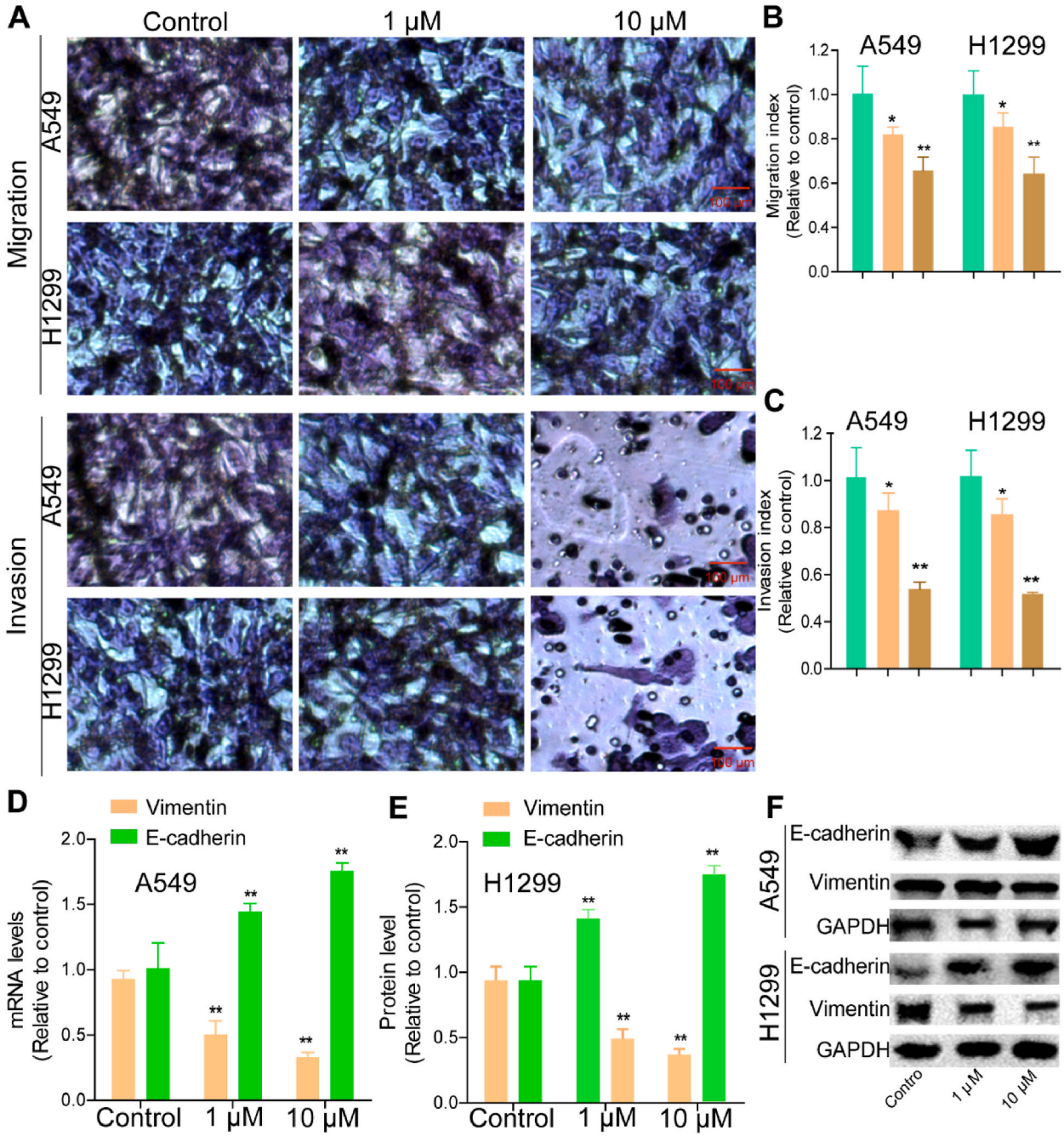

Fig. 2. Butyrate inhibits the migration and invasion ability of lung cancer cells. (A–C) The migration and invasion ability of A549 and H1299 cells was determined after being treated with the different concentrations of butyrate, and quantified in (B) and (C). (D–F) The expression of EMT markers was measured in the cells described in (A). *P < 0.05, **P < 0.01 vs control group.

Additionally, utilizing Extreme Limiting Dilution Analysis (ELDA), we observed that the frequency of CSCs in tumors derived from butyrate-treated cells was lower compared to that in tumors derived from control cells (Fig. 3C and D, Fig. 3G and H). This provides further evidence of butyrate's inhibitory effect on tumor initiation and underscores its potential in targeting the CSC population *in vivo*.

3.4. Butyrate suppresses the metastatic ability of lung cancer cells in vivo

Further *in vivo* studies were conducted to provide evidence of the metastasis-suppressive properties of butyrate. A549 and H1299 cells were intravenously injected into mice, followed by a 21-day butyrate treatment. Subsequently, the lung tissues of mice were

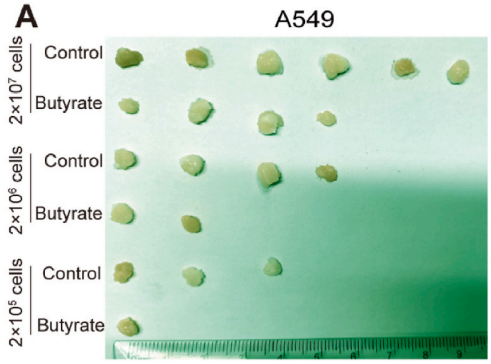

B

Injected cell number	Control	Butyrate
2×10^7	6/6	4/6
2×10^6	4/6	2/6
2×10^5	3/6	1/6

C

Confidence intervals for 1/(stem cell frequency)

Group	Lower	Estimate	Upper
Control	1349138	553366	226970
Butyrate	13801174	5708947	2361544

D

Overall test for differences in stem cell frequencies between any of groups

Chisq	DF	P.value
14.9	1	0.000116

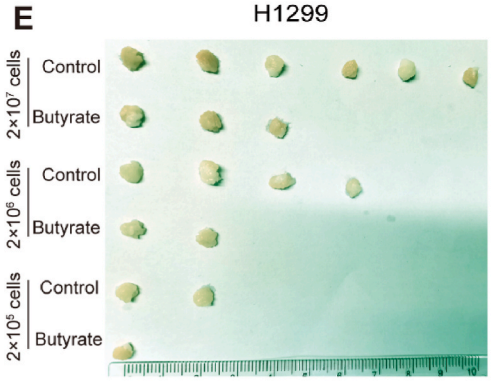

F

Injected cell number	Control	Butyrate
2×10^7	6/6	3/6
2×10^6	4/6	2/6
2×10^5	2/6	1/6

G

Confidence intervals for 1/(stem cell frequency)

Group	Lower	Estimate	Upper
Control	1652308	669540	271308
Butyrate	19857679	7929131	3166086

H

Overall test for differences in stem cell frequencies between any of groups

Chisq	DF	P.value
15.1	1	1e-04

Fig. 3. Butyrate attenuates the stemness of lung cancer cells *in vivo*. (A) The tumor images formed by different concentrations of A549 cells with or without butyrate treatment. (B) The formation ratio was calculated based on the data presented in (A). (C) The 1/(stem cell frequency) was calculated based on the results of (A) and (B) through the ELDA analysis. (D) The overall test for differences in stem cell frequencies between the control and butyrate group was detected through the ELDA analysis. (E) The tumor images formed by different concentrations of H1299 cells with or without butyrate treatment. (F) The formation ratio was calculated based on the data presented in (E). (G) The 1/(stem cell frequency) was calculated based on the results of (E) and (F) through the ELDA analysis. (H) The overall test for differences in stem cell frequencies between the control and butyrate group was detected through the ELDA analysis.

isolated and subjected to HE staining to observe lung metastatic nodes. Tumor xenografts treated with butyrate exhibited a decreased metastatic potential compared to control groups, as evidenced by larger metastatic nodes in mice without butyrate treatment (Fig. 4A) and a reduction in the number of metastatic nodes (Fig. 4B) with butyrate treatment. Consistently, flow cytometry analysis on the CD133+ subpopulation with stemness revealed that butyrate significantly reduced the ratio of CD133+ subpopulation in lung tissues (Fig. 4C and D). These results indicate that butyrate can selectively target lung CSCs and attenuate the stemness of lung cancer cells.

3.5. *Butyrate enhances the chemotherapeutic sensitivity of lung cancer cells in vitro and in vivo*

Given that the presence of CSCs is a recognized contributor to chemoresistance, we investigated whether butyrate could modulate the chemotherapeutic sensitivity of lung cancer cells through both *in vitro* and *in vivo* experiments. *In vitro* experiments revealed an increased susceptibility of lung cancer cells to cisplatin following exposure to butyrate (Fig. 5A and B). This effect was further validated *in vivo*, where tumor xenografts treated with a combination of butyrate and cisplatin demonstrated greater growth inhibition compared to groups treated with cisplatin alone, as evidenced by the reduction in tumor volume, size, and weight (Fig. 5C – 5E). Notably, the reduced weight observed in mice treated with cisplatin alone was mitigated by concurrent butyrate treatment, indicating the protective effects of butyrate on the toxicity associated with cisplatin (Fig. 5F). These findings suggest that butyrate may enhance the therapeutic efficacy of cisplatin and alleviate its adverse effects, potentially offering a synergistic and protective role in combination therapy for lung cancer.

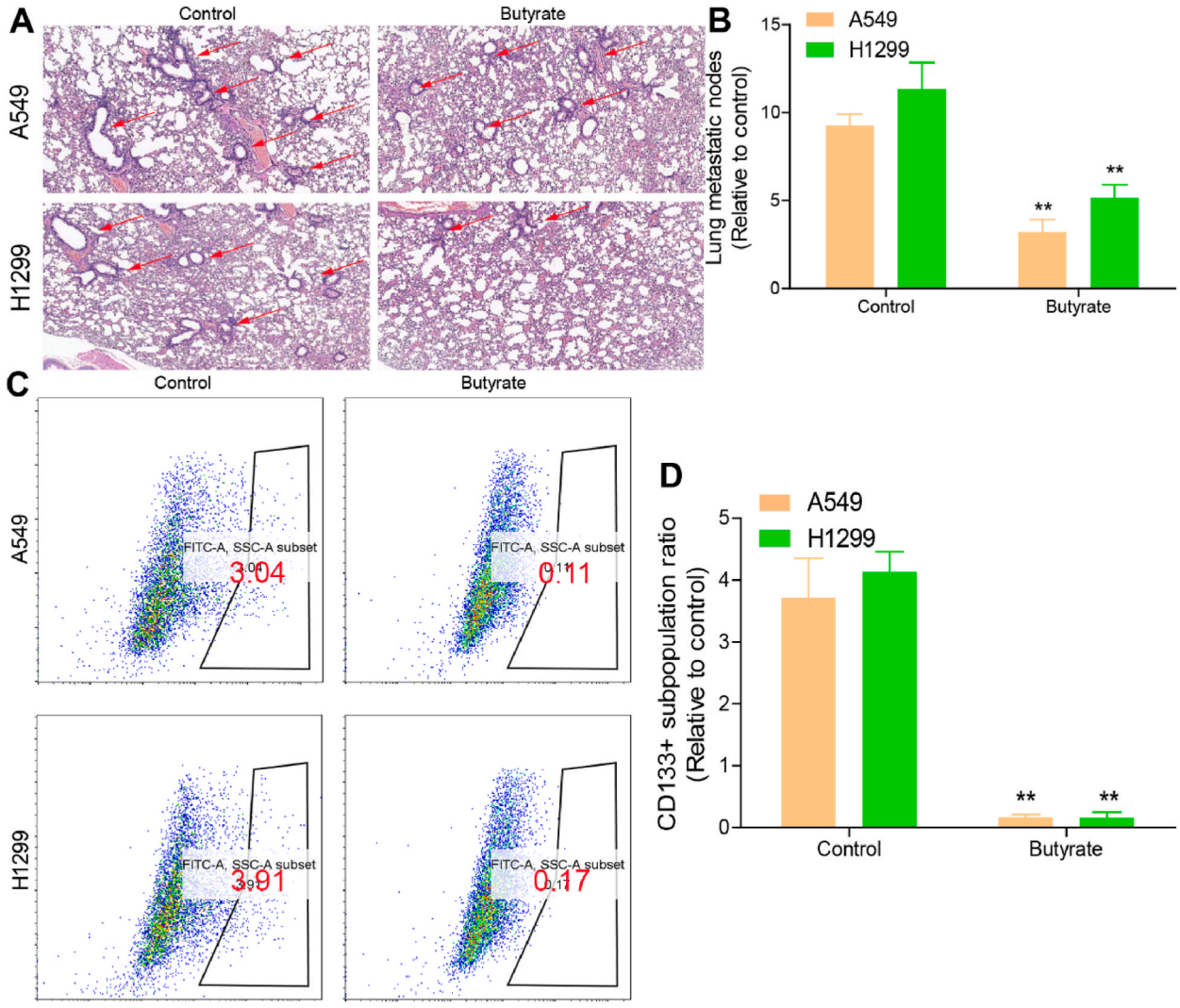

Fig. 4. Butyrate suppresses the metastatic ability of lung cancer cells *in vivo*. (A) The represented HE images for lung tissues derived from mice injected with lung cancer cells after being treated with butyrate for two weeks. (B) The metastatic nodes were measured in lung tissues derived from mice described in (A). (C and D) The CD133+ subpopulation in lung tissues derived from mice depicted in (A) was determined. **P < 0.01 vs control group.

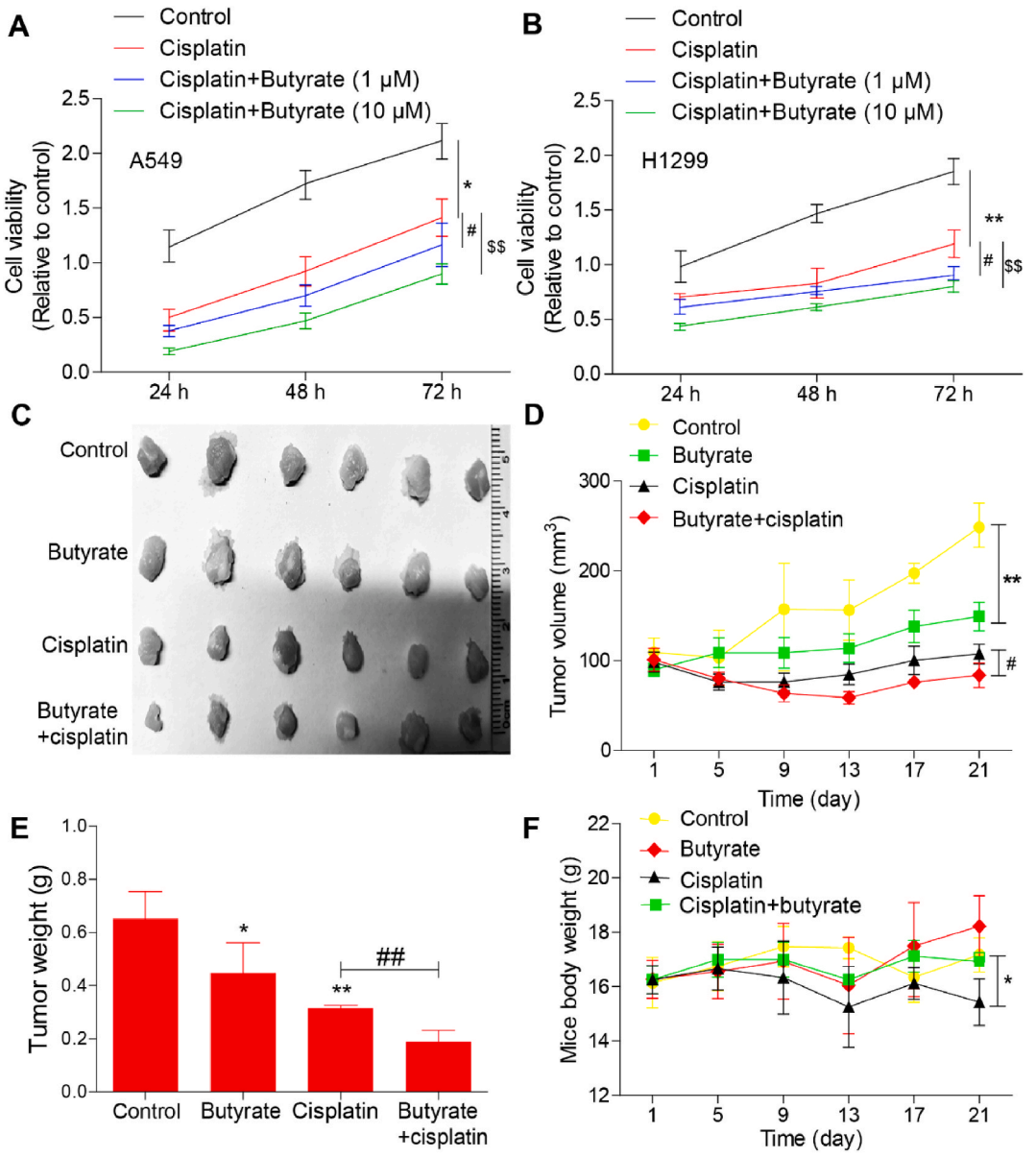

Fig. 5. Butyrate enhances the chemotherapeutic sensitivity of lung cancer cells *in vitro* and *in vivo*. (A and B) Cell viability was measured in A549 and H1299 cells treated with cisplatin as well as different concentrations of butyrate as indicated. **P < 0.01 vs control group, $^{\#}$P < 0.05 vs cisplatin group, $^{\$\$}$P < 0.01 vs cisplatin group. (C) Tumor images derived from A549 cells after the mice were treated with cisplatin (5 mg/kg), butyrate (10 mg/kg), or butyrate (5 mg/kg) + cisplatin (10 mg/kg) for three weeks. (D) Tumor volume was recorded for mice described in (C). **P < 0.01 vs control group, $^{\#}$P < 0.05 vs cisplatin group. (E) Tumor weight was measured for mice depicted in (C). *P < 0.05, **P < 0.01 vs control group, $^{\#\#}$P < 0.01 vs cisplatin group. (F) The weight of mice described in (C) was measured. *P < 0.05 vs cisplatin group.

3.6. Butyrate can recruit Fe2+ in lysosomes and decrease SLC7A11 protein stability via mediating the ubiquitination-lysosome degradastion

Mechanistically, we delved into the subcellular localization of butyrate and its role in modulating ferroptosis-related factors. IF analysis unveiled that butyrate predominantly localized to lysosomes, with minimal presence in mitochondria and cell membranes (Fig. 6A). Significantly, butyrate treatment led to the recruitment of Fe2+ within lysosomes (Fig. 6B), implying a potential link between butyrate and iron homeostasis. Given that GSH and iron concentration are pivotal regulators of lipid peroxides, critical contributors to ferroptosis, we further assessed the effects of butyrate on GSH levels in lung cancer cells. Interestingly, we found no significant change in GSH levels in lung cancer cells treated with butyrate (Fig. 6C). Moreover, we demonstrated that butyrate induced a cytoplasmic deletion of iron, characterized by increased expression of TfR1, IRP2, and DMT1 (divalent-metal transporter-1), along

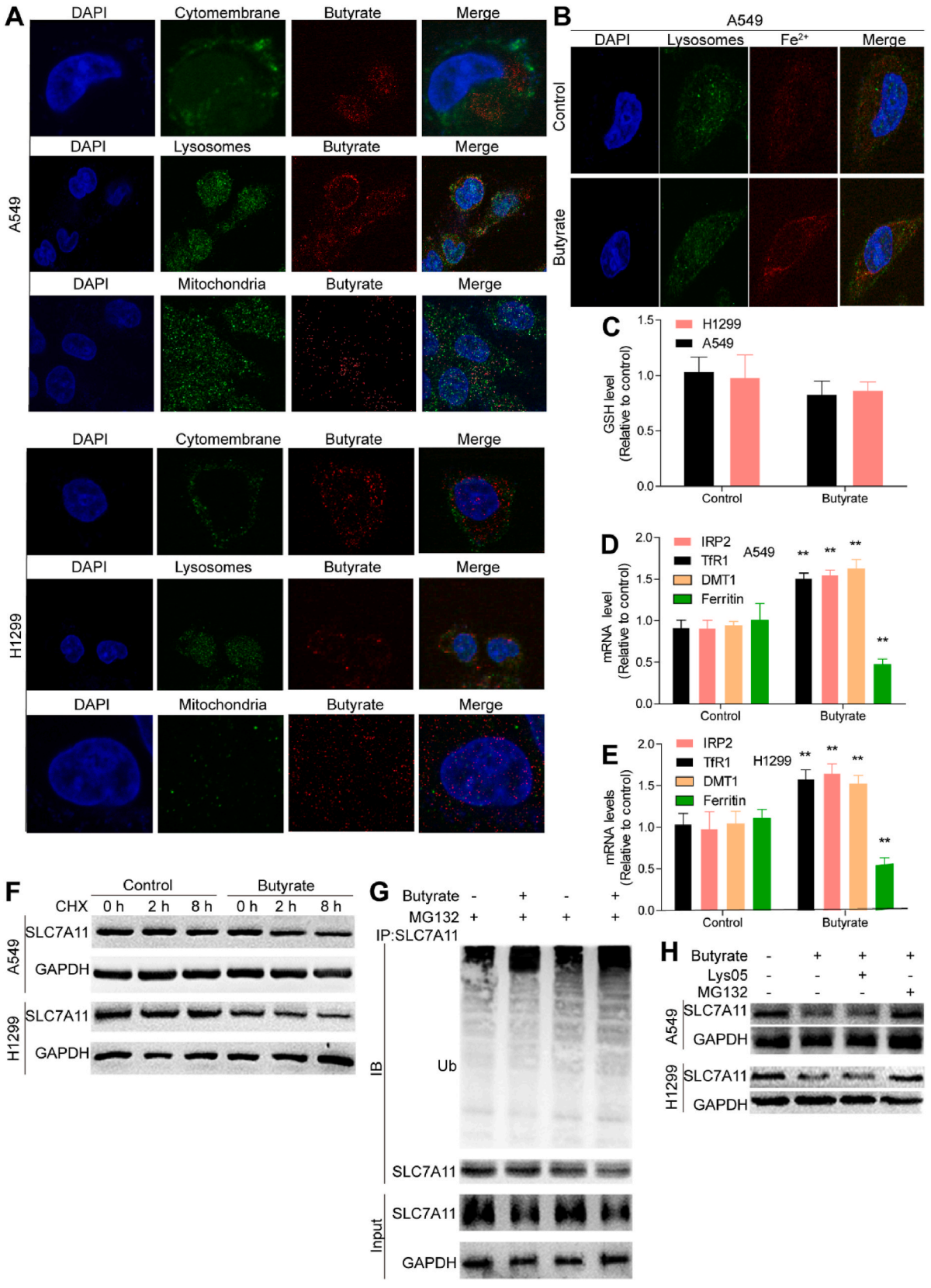

(caption on next page)

Fig. 6. Butyrate can recruit Fe^{2+} in lysosomes and decrease SLC7A11 protein stability via mediating the ubiquitination-lysosome degradation. (A) The localization of butyrate was detected in A549 and H1299 cells. (B) The concentration of Fe^{2+} was examined in A549 cells with or without butyrate treatment. (C) GSH level was determined in A549 cells with or without butyrate treatment. (D and E) The mRNA levels of IRP2, TfR1, DMT1, and Ferritin were evaluated in lung cancer cells with or without butyrate treatment. (F) The protein stability of SLC7A11 was measured in lung cancer cells with or without butyrate treatment. (G) The ubiquitination level of SLC7A11 was detected in A549 cells with or without butyrate treatment. (H) The protein level of SLC7A11 was examined in A549 lung cancer cells treated with butyrate as well as Lys05 or MG132.

with decreased ferritin expression (Fig. 6D and E). Additionally, we observed that the protein stability of SLC7A11 was reduced by butyrate treatment (Fig. 6F), and the ubiquitination level of SLC7A11 protein was significantly increased (Fig. 6G). Notably, the decrease of SLC7A11 protein induced by butyrate treatment was rescued by the proteasome inhibitor (MG132), but not by the lysosome inhibitor (Lys05) (Fig. 6H). This indicates the degradation of SLC7A11 protein via ubiquitination and proteasome-mediated pathways, contributing to the regulation of ferroptosis-associated processes.

3.7. Butyrate-mediated effects on lung CSCs are dependent on lysosome Fe^{2+}- and SLC7A11-mediated ferroptosis

Finally, we wondered whether butyrate-mediated effects on lung CSCs are indeed dependent on lysosome Fe^{2+}- and SLC7A11-mediated ferroptosis. To ascertain whether other cell death pathways, including apoptosis and necrosis, contribute to these effects, we introduced specific inhibitors — Nec-1 for necrosis, Z-VAD-FMK for apoptosis, and Fer-1 for ferroptosis — into lung cancer cells with butyrate treatment. As depicted in Fig. 7A and B, while the inhibition of apoptosis or necrosis could rescue the effects of butyrate on the sphere-formation ability of lung cancer cells, it did not exhibit significance. However, ferroptosis inhibitor Fer-1 partially reversed the inhibition of butyrate on the sphere-formation ability of lung cancer cells. Additionally, overexpression of SLC7A11 also rescued butyrate-mediated suppression of the sphere-formation ability of lung cancer cells (Fig. 7C and D). Furthermore, consistent results were obtained when examining the CD133+ subpopulation with stemness (Fig. 7E and F). Moreover, the butyrate-mediated reduction in ALDH activity and CSC markers expression was attenuated by Fer-1 and SLC7A11 overexpression (Fig. 7G – 7I). Collectively, these results demonstrate that butyrate can suppress lung cancer stemness, relying on lysosome Fe^{2+}- and SLC7A11-mediated ferroptosis.

4. Discussion

In this study, we have elucidated the novel and distinctive aspects of butyrate-induced ferroptosis in lung CSCs, shedding light on several key areas that demonstrate the uniqueness of our findings. Our research contributes to a deeper understanding of the interplay between butyrate, ferroptosis, and lung CSCs, with implications for innovative therapeutic strategies. We will delve into the following pivotal points in a structured manner, highlighting their significance, mechanisms, and implications.

One of the most noteworthy findings of our study is the selective suppression of lung CSCs by butyrate treatment. This unique effect stands in contrast to traditional chemotherapy agents that often target both cancerous and healthy cells indiscriminately. By specifically inhibiting the viability and stemness of lung CSCs, butyrate presents an innovative therapeutic avenue that addresses a critical challenge in lung cancer treatment – the eradication of treatment-resistant CSC populations. While prior research has explored the role of butyrate in various cancer models [24–26], our study significantly advances this knowledge by specifically highlighting its impact on CSCs. This distinctive aspect underscores the potential of butyrate as a targeted therapeutic agent with the ability to disrupt the driving force behind tumor progression.

Our exploration into the underlying mechanisms of butyrate-induced ferroptosis uncovers a unique interplay between butyrate, lysosomal iron recruitment, and the regulation of SLC7A11 protein stability. While ferroptosis has been a subject of interest, the novel contribution of our study lies in uncovering the role of butyrate in modulating iron homeostasis within lysosomes. The preferential localization of butyrate in lysosomes, along with its ability to recruit Fe2+, highlights a potential pathway for disrupting iron metabolism and enhancing lipid peroxidation-driven cell death. Similar mechanisms have been elucidated in previous studies [4,5,27–29], leading us to speculate that recruiting Fe^{2+} might be potential target for CSCs and, consequently, tumor treatment. Furthermore, the identification of a regulatory pathway involving the ubiquitination and lysosomal degradation of SLC7A11 protein presents a novel approach to sensitize CSCs to ferroptosis induction [30–32]. This unique mechanistic insight enriches the understanding of how butyrate can orchestrate ferroptotic processes, laying a solid foundation for further investigations and potential therapeutic interventions.

Our study goes beyond observing correlations and causations, delving into the dependency relationship between the effects of butyrate on lung CSCs and the lysosome Fe^{2+}- and SLC7A11-mediated ferroptosis pathway. While the link between ferroptosis and CSCs has been acknowledged, our research bridges the gap between the effects of butyrate and its influence on ferroptosis induction in CSCs. This linkage is not only unique but also essential in substantiating the potential of butyrate as a targeted CSC therapy. The results from our experiments employing ferroptosis inhibitors and SLC7A11 overexpression underscore the direct relationship between butyrate's actions and its influence on the ferroptosis pathway. This novel insight strengthens the rationale for exploring butyrate-mediated ferroptosis as a therapeutic strategy for targeting lung CSCs. However, while this study offers valuable insights into the potential therapeutic implications of butyrate in targeting lung CSCs through lysosome Fe2+- and SLC7A11-mediated ferroptosis, a more comprehensive elucidation is needed to underscore the significance of these findings for lung cancer treatment. Expanding on how this research advances the current understanding of lung cancer pathogenesis and treatment strategies, as well as exploring the

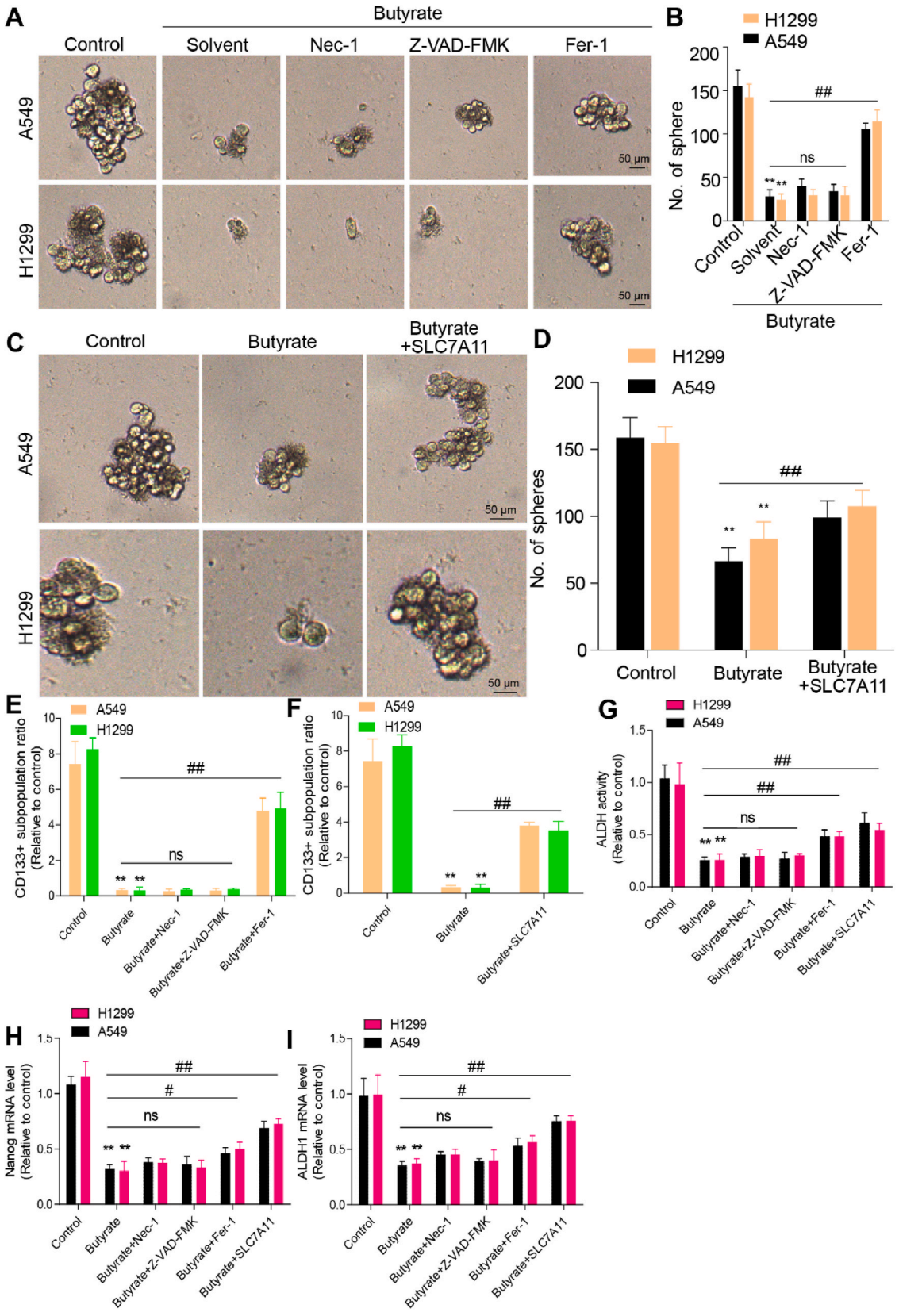

(caption on next page)

Fig. 7. Butyrate-mediated effects on lung CSCs are dependent on lysosome Fe^{2+}- and SLC7A11-mediated ferroptosis. (A and B) The sphere size and number were detected in lung cancer cells with different treatment as indicated. (C and D) The sphere size and number were examined in lung cancer cells with butyrate treatment as well SLC7A11 overexpression or not. (E) The CD133+ subpopulation was measured in cells described in (A). (F) The CD133+ subpopulation was determined in cells described in (C). (G) ALDH1 activity was measured in cells described in (A and C). (H and I) The mRNA levels of Nanog and ALDH1 was detected in lung cancer cells described in (A and C). $^{**}P < 0.01$ vs control group, $^{\#\#}P < 0.01$ vs butyrate group, ns means no significance.

translational aspects leading to the development of novel therapeutic interventions or potential clinical applications, would augment the overall impact of the study. Additionally, the study primarily focuses on ferroptosis as the mode of cell death induced by butyrate. Other inhibiting other cell death pathways could not rescue the effects of butyrate on the sphere-formation ability of lung cancer cells, they also should be considered, as their roles in lung cancer progression might influence the overall outcomes. Furthermore, the study primarily focuses on short-term effects of butyrate treatment. Investigating the long-term consequences, especially regarding potential resistance mechanisms or sustained therapeutic effects, would provide a more comprehensive view.

In conclusion, our study has made significant contributions by elucidating the selectively suppression of lung CSCs through butyrate-induced ferroptosis and providing mechanistic insights into the underlying processes. The distinctive aspects we discussed – preferential targeting, unique mechanisms, and pathway dependence – collectively highlight the transformative potential of butyrate as a modulator of ferroptosis in lung CSCs.

Ethics statement

The Institutional Review Board of Xinhua Hospital Affiliated to Shanghai Jiao Tong University School of Medicine approves this project to be carried according to designed (XHEC-F-2023-064).

Data availability statement

All data generated or analyzed during this study are included in this published article.

CRediT authorship contribution statement

Rui Bi: Formal analysis. **Lianyong Jiang:** Investigation, Data curation. **Rui Hu:** Methodology, Investigation. **Bohan Wen:** Resources, Methodology. **Zhaolei Jiang:** Validation, Supervision, Software. **Hongtao Liu:** Validation, Supervision. **Ju Mei:** Writing – review & editing, Visualization, Supervision.

Declaration of competing interest

The authors declare that they have no known competing financial interests or personal relationships that could have appeared to influence the work reported in this paper.

Acknowledgements

Not applicable.

Appendix ASupplementary data

Supplementary data to this article can be found online at https://doi.org/10.1016/j.heliyon.2024.e28093.

References

[1] M. Oudkerk, S. Liu, M.A. Heuvelmans, J.E. Walter, J.K. Field, Lung cancer LDCT screening and mortality reduction - evidence, pitfalls and future perspectives, Nat. Rev. Clin. Oncol. 18 (3) (2021) 135–151.
[2] X. Zhou, R. Zhou, X. Rao, J. Hong, Q. Li, X. Jie, J. Wang, Y. Xu, K. Zhu, Z. Li, et al., Activated amino acid response pathway generates apatinib resistance by reprograming glutamine metabolism in non-small-cell lung cancer, Cell Death Dis. 13 (7) (2022) 636.
[3] G. Lei, L. Zhuang, B. Gan, Targeting ferroptosis as a vulnerability in cancer, Nat. Rev. Cancer 22 (7) (2022) 381–396.
[4] Y. Yang, Y. Lu, C. Zhang, Q. Guo, W. Zhang, T. Wang, Z. Xia, J. Liu, X. Cheng, T. Xi, et al., Phenazine derivatives attenuate the stemness of breast cancer cells through triggering ferroptosis, Cell. Mol. Life Sci. : CMLS 79 (7) (2022) 360.
[5] T.T. Mai, A. Hamai, A. Hienzsch, T. Caneque, S. Muller, J. Wicinski, O. Cabaud, C. Leroy, A. David, V. Acevedo, et al., Salinomycin kills cancer stem cells by sequestering iron in lysosomes, Nat. Chem. 9 (10) (2017) 1025–1033.
[6] H. Ni, H. Qin, C. Sun, Y. Liu, G. Ruan, Q. Guo, T. Xi, Y. Xing, L. Zheng, MiR-375 reduces the stemness of gastric cancer cells through triggering ferroptosis, Stem Cell Res. Ther. 12 (1) (2021) 325.
[7] R.I. Henkin, Clinical and therapeutic implications of cancer stem cells, N. Engl. J. Med. 381 (10) (2019) e19.

[8] B. Zhao, X. Li, Y. Wang, P. Shang, Iron-dependent cell death as executioner of cancer stem cells, Journal of experimental & clinical cancer research : CR 37 (1) (2018) 79.
[9] Y. Yang, X. Li, T. Wang, Q. Guo, T. Xi, L. Zheng, Emerging agents that target signaling pathways in cancer stem cells, J. Hematol. Oncol. 13 (1) (2020) 60.
[10] Szentirmai É, N.S. Millican, A.R. Massie, L. Kapás, Butyrate, a metabolite of intestinal bacteria, enhances sleep, Sci. Rep. 9 (1) (2019) 7035.
[11] J.R. Lupton, Butyrate and colonic cytokinetics: differences between in vitro and in vivo studies, Eur. J. Cancer Prev. : the official journal of the European Cancer Prevention Organisation (ECP) 4 (5) (1995) 373–378.
[12] Y. He, Y. Ling, Z. Zhang, R.T. Mertens, Q. Cao, X. Xu, K. Guo, Q. Shi, X. Zhang, L. Huo, et al., Butyrate reverses ferroptosis resistance in colorectal cancer by inducing c-Fos-dependent xCT suppression, Redox Biol. 65 (2023) 102822.
[13] K.S. Fluitman, M. Wijdeveld, M. Nieuwdorp, Rg Ij, Potential of butyrate to influence food intake in mice and men, Gut 67 (7) (2018) 1203–1204.
[14] S. Sitkin, T. Vakhitov, J. Pokrotnieks, Oral butyrate modulates the gut microbiota in patients with inflammatory bowel disease, most likely by reversing proinflammatory metabolic reprogramming of colonocytes, Neuro Gastroenterol. Motil. 33 (1) (2021) e14038.
[15] R. Bi, R. Hu, L. Jiang, B. Wen, Z. Jiang, H. Liu, J. Mei, Butyrate enhances erastin-induced ferroptosis of lung cancer cells via modulating the ATF3/SLC7A11 pathway, Environ. Toxicol. 39 (2) (2024) 529–538.
[16] Y. Zhao, J. Li, W. Guo, H. Li, L. Lei, Periodontitis-level butyrate-induced ferroptosis in periodontal ligament fibroblasts by activation of ferritinophagy, Cell death discovery 6 (1) (2020) 119.
[17] G. Wang, S. Qin, L. Chen, H. Geng, Y. Zheng, C. Xia, J. Yao, L. Deng, Butyrate dictates ferroptosis sensitivity through FFAR2-mTOR signaling, Cell Death Dis. 14 (4) (2023) 292.
[18] Z. Bian, X. Sun, L. Liu, Y. Qin, Q. Zhang, H. Liu, L. Mao, S. Sun, Sodium butyrate induces CRC cell ferroptosis via the CD44/SLC7A11 pathway and exhibits a synergistic therapeutic effect with erastin, Cancers 15 (2) (2023).
[19] J. Hou, J. Xu, Y. Liu, H. Zhang, S. Wang, Y. Jiao, L. Guo, S. Li, Sodium butyrate inhibits osteogenesis in human periodontal ligament stem cells by suppressing smad1 expression, BMC Oral Health 22 (1) (2022) 301.
[20] S. Rashid, A. Salim, R. Qazi, T.S. Malick, K. Haneef, Sodium butyrate induces hepatic differentiation of mesenchymal stem cells in 3D collagen scaffolds, Appl. Biochem. Biotechnol. 194 (8) (2022) 3721–3732.
[21] A. Satheesan, S. Sharma, A. Basu, Sodium butyrate induced neural stem/progenitor cell death in an experimental model of Japanese encephalitis, Metab. Brain Dis. 38 (8) (2023) 2831–2847.
[22] L. Zheng, Q. Guo, C. Xiang, S. Liu, Y. Jiang, L. Gao, H. Ni, T. Wang, Q. Zhao, H. Liu, et al., Transcriptional factor six2 promotes the competitive endogenous RNA network between CYP4Z1 and pseudogene CYP4Z2P responsible for maintaining the stemness of breast cancer cells, J. Hematol. Oncol. 12 (1) (2019) 23.
[23] Y. Zhou, Z. Han, Z. Zhao, J. Zhang, Scoparone attenuates glioma progression and improves the toxicity of temozolomide by suppressing RhoA/ROCK1 signaling, Environ. Toxicol. 39 (2) (2024) 562–571.
[24] W. Wei, W. Sun, S. Yu, Y. Yang, L. Ai, Butyrate production from high-fiber diet protects against lymphoma tumor, Leuk. Lymphoma 57 (10) (2016) 2401–2408.
[25] C. Panebianco, A. Villani, F. Pisati, F. Orsenigo, M. Ulaszewska, T.P. Latiano, A. Potenza, A. Andolfo, F. Terracciano, C. Tripodo, et al., Butyrate, a postbiotic of intestinal bacteria, affects pancreatic cancer and gemcitabine response in *in vitro* and in vivo models, Biomedicine & pharmacotherapy = Biomedecine & pharmacotherapie 151 (2022) 113163.
[26] J. Kang, M. Sun, Y. Chang, H. Chen, J. Zhang, X. Liang, T. Xiao, Butyrate ameliorates colorectal cancer through regulating intestinal microecological disorders, Anti Cancer Drugs 34 (2) (2023) 227–237.
[27] J. Lv, Z. Wang, H. Liu, Erianin suppressed lung cancer stemness and chemotherapeutic sensitivity via triggering ferroptosis, Environ. Toxicol. 39 (2) (2024) 479–486.
[28] Y. Xu, Q. Wang, X. Li, Y. Chen, G. Xu, Itraconazole attenuates the stemness of nasopharyngeal carcinoma cells via triggering ferroptosis, Environ. Toxicol. 36 (2) (2021) 257–266.
[29] J. Sun, X. Cheng, S. Pan, L. Wang, W. Dou, J. Liu, X. Shi, Dichloroacetate attenuates the stemness of colorectal cancer cells via trigerring ferroptosis through sequestering iron in lysosomes, Environ. Toxicol. 36 (4) (2021) 520–529.
[30] B. Zhang, W. Bao, S. Zhang, B. Chen, X. Zhou, J. Zhao, Z. Shi, T. Zhang, Z. Chen, L. Wang, et al., LncRNA HEPFAL accelerates ferroptosis in hepatocellular carcinoma by regulating SLC7A11 ubiquitination, Cell Death Dis. 13 (8) (2022) 734.
[31] F. Lin, W. Chen, J. Zhou, J. Zhu, Q. Yao, B. Feng, X. Feng, X. Shi, Q. Pan, J. Yu, et al., Mesenchymal stem cells protect against ferroptosis via exosome-mediated stabilization of SLC7A11 in acute liver injury, Cell Death Dis. 13 (3) (2022) 271.
[32] Q. Chen, W. Zheng, J. Guan, H. Liu, Y. Dan, L. Zhu, Y. Song, Y. Zhou, X. Zhao, Y. Zhang, et al., SOCS2-enhanced ubiquitination of SLC7A11 promotes ferroptosis and radiosensitization in hepatocellular carcinoma, Cell Death Differ. 30 (1) (2023) 137–151.